January 1999

# Methods for Modeling and Predicting Mechanical Deformations of the Breast During Interventional Procedures

Fred S. Azar
*University of Pennsylvania*

Dimitris N. Metaxas
*University of Pennsylvania*

Reid T. Miller
*Exponent Failure Analysis Associates*

Mitchell D. Schnall
*University of Pennsylvania*, Schnall@oasis.rad.upenn.edu



University of Pennsylvania Department of Computer and Information Science Technical Report No. MS-CIS-99-13.

# Methods for Modeling and Predicting Mechanical Deformations of the Breast During Interventional Procedures

**Abstract**
When doing high field (1.5T) magnetic resonance breast imaging, the use of compression plate during imaging after a contrast-agent injection may critically change the enhancement characteristics of the tumor, making the tracking of its boundaries very difficult. A new method for clinical breast biopsy is presented based on a deformable finite element model of the breast. The geometry of the model is constructed from MR data, and its mechanical properties are based on a non-linear material model. This method allows imaging the breast without compression before the procedure, then compressing the breast and using the finite element model to predict the tumor's position. The axial breast contours and the segmented slices are ported to a custom-written MR-image contour analysis program, which generates a finite element model (FEM) input file readable by a commercial FEM software. A deformable silicon gel phantom was built to study the movements of an inclusion inside a deformable environment. The hyperelastic properties of the phantom materials were evaluated on an Instron Model 1331 mechanical testing machine. The phantom was placed in a custom-built pressure device, where a pressure plate caused a 14% (9.8mm) compression. The phantom was imaged in a 1.5T magnet (axial and coronal), in the undeformed and deformed states. An FEM of the phantom was built using the custom-written software from the MR data, and another FEM of the phantom was built using a commercial pre-processor from the phantom's directly measured dimensions. The displacements of the inclusion center and its boundaries were calculated, both from the experimental and FEM results. The calculated displacements from both models are within 0.5mm of each other, and agree within 1.0mm with the experimental results. This difference is within the imaging error.

**Comments**
University of Pennsylvania Department of Computer and Information Science Technical Report No. MS-CIS-99-13.

# Methods for Modeling and Predicting Mechanical Deformations of the Breast during Interventional Procedures

Fred S. Azar[1], Dimitris N. Metaxas[2], Reid T. Miller[3], Mitchell D. Schnall[4]

[1]Dept. of BioEngineering, University of Pennsylvania, 411 Blockley Hall, 4th floor ,
423 Guardian Dr., Philadelphia PA 19104
fredazar@seas.upenn.edu
[2]Dept. of Computer Science, University of Pennsylvania
dnm@graphics.cis.upenn.edu
[3]Exponent Failure Analysis Associates, 2300 Chestnut, Philadelphia PA 19103
[4]Department of Radiology, Hospital of the University of Pennsylvania, MRI Bldg.
1 Founders, 3400 Spruce St., Philadelphia PA 19104
schnall@oasis.rad.upenn.edu

Technical Report MS-CIS-99-13
MS-BE-00-03
Dept. of BioEngineering, U. of Pennsylvania
1999

**Abstract.** When doing high field (1.5T) magnetic resonance breast imaging, the use of a compression plate during imaging after a contrast-agent injection may critically change the enhancement characteristics of the tumor, making the tracking of its boundaries very difficult. A new method for clinical breast biopsy is presented, based on a deformable finite element model of the breast. The geometry of the model is constructed from MR data, and its mechanical properties are based on a non-linear material model. This method allows imaging the breast without compression before the procedure, then compressing the breast and using the finite element model to predict the tumor's position. The axial breast contours and the segmented slices are ported to a custom-written MR-image contour analysis program, which generates a finite element model (FEM) input file readable by a commercial FEM software. A deformable silicone gel phantom was built to study the movement of an inclusion inside a deformable environment. The hyperelastic properties of the phantom materials were evaluated on an Instron Model 1331 mechanical testing machine. The phantom was placed in a custom-built pressure device, where a pressure plate caused a 14% (9.8mm) compression. The phantom was imaged in a 1.5T magnet (axial and coronal), in the undeformed and deformed states. An FEM of the phantom was built using the custom-written software from the MR data, and another FEM of the phantom was built using a commercial pre-processor from the phantom's directly measured dimensions. The displacements of the inclusion center and its boundaries were calculated, both from the experimental and FEM results. The calculated displacements from both models are within 0.5mm of each other, and agree within 1.0mm with the experimental results. This difference is within the imaging error.

## 1 Introduction

It is impossible today to do continuous breast imaging using High Field (1.5T) Superconducting Magnetic Resonance imaging. Moreover, the use of compression plates when imaging the breast

after injection of a contrast agent may change the enhancement characteristics of the tumor and could make the lesion disappear, making the tracking of tumor boundaries very difficult.
We present a new method for clinical breast biopsy and/or surgery guidance, based on the use of a deformable finite element breast model whose geometry is constructed from MR data. The material properties of the deformable model are based on a nonlinear material model. This method allows to image the breast without any compression before a needle procedure, then compress the breast, and its finite element model (by applying the same pressure to both). The position of tumor in the real breast before the biopsy can then be identified by finding the position of the tumor in the compressed finite element model.
First, the breast model is described from obtaining the breast MR data, to creating the geometric model. The materials and methods then describe an initial silicon gel phantom study whose goal is to predict the movement of an inclusion inside a deformable environment (as the tumor in the breast), using the FEM of the silicon gel phantom. The results of the initial phantom study suggest that the compressed model may allow us to precisely track the position and motion of the tumor in the real compressed breast before inserting the needle.

# 1 Background and Motivation

Breast cancer is the most commonly diagnosed cancer and the second leading cause of cancer death among American women [1]. Breast magnetic resonance imaging (MRI) has become a robust and valuable technique, with an almost unlimited sensitivity for detection of invasive breast cancer [2] [3]. However, without the use of a contrast-enhancing agent (such as gadolinium dimeglumine [4-6]), MRI is of little benefit to detect tumors in the breast [6-8].
It is generally accepted that the sensitivity of breast MRI for invasive breast cancers approaches 100% [7] (however the sensitivity for in situ cancer has been reported to vary dramatically between 40%and 100% [9] [10]).

An MR imaging-guided breast localization and biopsy system is thus needed to help differentiate between the benign enhancing lesions, and carcinomas. Lesion localization techniques described for use on a standard 1.5T system are based on the assumption that the appearance and shape of the potential lesion does not change during the entire procedure.

The MR imaging-guided localization techniques encounter the following problems:

- The appearance, size and shape of the potential cancer lesion greatly depends on dynamics of the contrast-enhancing agent. As explained above, the lesion may clearly appear only in the two minutes following the contrast agent injection, then the signal intensity may vary arbitrarily, and it is quite possible that the apparent boundaries of the lesion may change dramatically.
- The use of compression plates when imaging the breast after injection of the contrast-enhancing agent may change the enhancement characteristics of the tumor and could very well make the lesion disappear.
- The deformable nature of the breast makes it very difficult to stabilize, and both external movements (due to the patient), and internal deformations that occur as the needle is inserted.
- The compression plates could compress the breast to a degree that makes it virtually immobile, however this would cause a high level of discomfort to the patient in addition to the possible anxiety, in addition to the possible altered enhancement characteristics of the tumor as mentioned above.
- Furthermore, the guidance techniques all use static MR images for localizing the lesions (pre and then postcontrast). It is impossible today to do continuous breast imaging using high

field (1.5T) superconducting magnetic resonance imaging. Therefore live imaging can't be maintained throughout the entire procedure.

- When comparing MR-images and X-ray mammography images of the same breast in order to obtain more valuable information on the nature and localization of the lesion, there is no known technique that would register an image from one modality to the other. Due to the different position and deformation states of the breast in each modality (patient is standing straight for mammography, and lying prone for MR imaging), no simple deformation technique can be applied to register the corresponding images from the two modalities. Today the surgeon simply visually compares the images placed beside each other, and uses his/her best judgement to identify the same lesion in the two images.

The above limitations coupled with the deformable structure of the breast make needle procedures very sensitive to the initial placement of the needle. It thus becomes relatively uncertain that the tissue specimen removed during the biopsy procedure actually belongs to the lesion of interest. It now becomes imperative to develop a new technique, which would solve or bypass the aforementioned problems.
We present a new method for clinical breast biopsy and/or surgery guidance, based on the use of an accurate virtual finite element breast model of the patient, capable of modeling the deformation of the breast. The geometry of the model is constructed from MR data. The hyperelastic properties of the deformable model are based on a on nonlinear material model. This method will allow imaging of the breast without any compression before a needle procedure, then compress the breast, and its virtual finite element model (by applying the same deformation to both). Furthermore this model will allow data sets of the same breast from different imaging modalities to be correctly registered, by subjecting the virtual breast model to the same physical conditions as the real breast.
A finite element model of the breast will be a very flexible tool for many applications including those mentioned above, and also for diagnosis, measurements, surgery planning, simulations of deformation due to inserting a needle, and further away, virtual surgery, and even tele-surgery.

## 3 Physiology of the Breast

Fig. 1. shows the major structures of the breast. The dimensions and weight of the breast can greatly vary per individual. The mammary gland forms a cone with its base at the chest wall and its apex at the nipple. Normal skin thickness lies between 0.5 and 1mm. Breast skin thickness varies between large and small breasts. The superficial layer (fascia) is separated from the skin by 0.5 to 2.5 cm of subcutaneous fat. Tentacle-like prolongations of fibrous tissue extend in all directions from this fascia to the skin. In the adult mammary gland, there are 15 to 20 irregular lobes, converging to the nipple through ducts 2 to 4.5 mm in diameter [11]. These ducts are immediately surrounded by dense interlobular (myoepithelial cells) and intralobular connective tissue (containing few collagenous fibers). These fibrous sheaths are the supporting framework. Carcinomas in affected breasts are usually accompanied by local changes in material properties, due to increased density of the lesion, the shape and size of the lesion, and local skin thickening [12]. There are several types of breast cancer, however the most common are ductal carcinoma (which begins in the lining of the milk ducts of the breast), and lobular carcinoma (which begins in the lobules where breast milk is produced) [13].

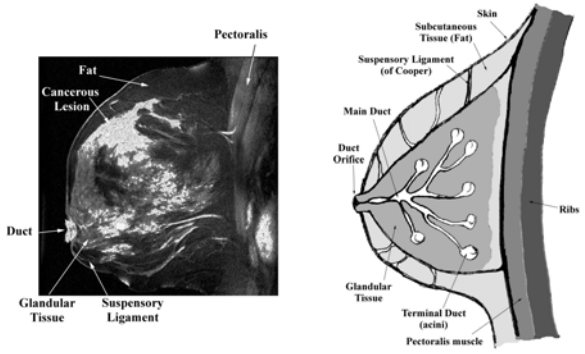


**Fig. 1.** Glandular and supporting framework of the breast.

Breast lesions that are relevant to this paper are those which usually necessitate a biopsy or removal: they are lumps of highly varying shapes, with diameters ranging from a few millimeters to several centimeters. That is why many lesions cannot be represented by a specific shape due to their physical extent, and particular nature.

## 4 Description of the Breast Model

The model of the breast is based on MR data. Because of the high variability of breast shapes and the deformation of the breast when compressed in order to be imaged, the model devised closely follows the contours of the patient breast.

### 4.1 Breast MR Data

The patient data is a set of parallel 2D spoiled gradient echo MR axial slices of the breast, using an axial T1-weighted sequence: they are called axial localizers, and are actually imaged before every examination to the breast. This makes the availability of such data very high and no additional scans are needed, to the benefit of the patient.

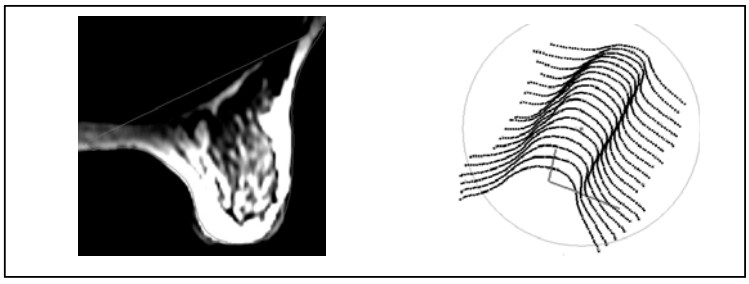

**Fig. 2.** Axial MR slice of breast from axial localizer (left) and breast contours (right).

The MR axial slices are then segmented. Using snakes, or any other contour method, the contour of each breast slice is drawn, from the medial side to the lateral side (as shown in Fig. 2 . Then the main structures (breast tissue, fat, and possibly cancerous tumor) are segmented, and and the

results are saved to a file for subsequent use. Based on the external set of 2D axial slices we obtain a series of parallel contours. When displayed in 3D, the breast contours appear as in Figure 2.
These contours represent the breast volume in which the surgeon will operate. The breast is compressed between two parallel plates, giving it the shape in Fig. 2.

### 4.2 Geometric Model

The breast contours (Fig. 2), and the segmented breast are ported to a custom-written MR-image contour analysis program, *BreastView*. Running on a Silicon Graphics (SGI) indigo2 machine, it generates the 3D computational domain (mesh) of the breast. The volume elements created from the mesh can be scaled to any size that fits the demands of the application. Then *BreastView* assigns to each volume element its corresponding material definition, based on the segmented data of the breast.
The program generates a finite element model (FEM) input file readable by a robust commercial FEM software such as ABAQUS (Hibbit, Karlsson & Sorensen, Rhode Island). Figure 3 shows a contour, and the 2D mesh generated in it.

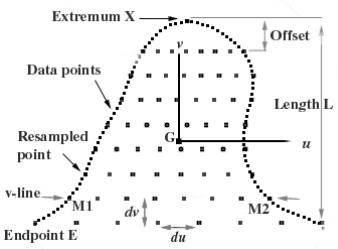


**Fig. 3.** Slice contour, and 2D mesh generated in the (u,v) coordinate system.

In order to create the 3D mesh, we first find the principal direction *d* (direction of the *v*-axis, Fig. 3), from the chest wall to the nipple. Any line with direction *d* in the plane of the contour, which intersects the contour, intersects it twice. This direction is that of the line orthogonal to the line which passes through the two endpoints (the principal direction method using the eigenvectors of the contour set of points did not yield the best direction *d*). The center of gravity G of the contour set is calculated. The 3D mesh can now be easily generated following the U and V resolution desired, in the orthogonal *u,v* basis centered at G. This algorithm ensures that we have the same number of points on every V-line, and the same number of V-lines on every slice.
The 3D volume elements are solid quadrilateral trilinear isoparametric elements, except at the tip of the mesh, where the volume elements are pyramidal. The skin is modeled as 2D membrane elements which have low axial stiffness, but non-linear elastic behavior in the plane of the elements. The software *BreastView* permits the mesh to be as dense as needed.

## 5 Materials and Methods

A silicone gel phantom can be used to study to movement of an inclusion inside a deformable environment (as tumor inside the breast), and also to validate the model. The phantom can have magnetic properties (T1 and T2) similar to those of human breast tissue, and in such a way as to produce a good signal to noise ratio. An initial study was conducted using such a phantom. The phantom was designed to withstand large deformations (20% or greater), and to enable controlled deformations. A silicon inclusion was inserted in the phantom, which is 4.3 times stiffer than the surrounding silicon. The phantom was imaged undeformed, then compressed. A 3D deformable

model of the phantom was built from the resulting MR data using the custom-written software *BreastView*. Another FEM of the phantom was also built from its directly measured dimensions using a commercial pre-processor program. This latter model can be used to assess the inaccuracies introduced in the former model due to errors in dimension measurements from the MR images. The displacement vectors of the 8 corners of the stiff phantom inclusion and its center, were measured both from the MR images and from the finite element models.

### 5.1 Phantom construction

The gel phantom was build using the Sylgard Primerless Dielectric Gel 527 (Dow Corning, Midland, Mich.). The gel system is composed of two parts, catalyst (part A) and resin (part B), the ratio of which determines its elastic properties (a decrease in A:B produces stiffer gels). The MR signal is derived entirely from methyl protons (the dependence of T1 and T2 on A:B is examined in [14]). A similar silicon gel (model Q7-2218, Dow Corning) has been suggested for use in MR imaging [14], and the same silicone gel was used to validate tagging with MR imaging to estimate material deformation [15].
The geometry of the deformable phantom consists of a rectangular box containing a rectangular inclusion, with the dimensions as shown in Fig. 4.

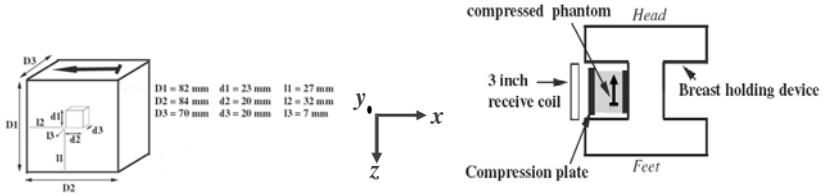


(a) (b)

**Fig. 4.** (a) Geometry of the silicone gel phantom, (b) Top view of the setup for imaging the compressed silicone gel phantom.

### 5.2 MR imaging

The full silicone gel phantom was placed in a custom-built pressure device, where a pressure plate could compress the gel phantom in a similar way as with a real breast with the desired amount of deformation. The phantom was placed in the breast holding device as shown in Fig. 4. The compression plate was placed parallel to the phantom so it would compress it from the top, down a distance of 7.2 cm. This left an uncompressed height of 1.0cm. The whole setup was secured firmly and imaged with a whole body 1.5 T superconducting magnet (Signa; GE Medical Systems, Milwaukee, Wis.).
The silicone gel phantom was first imaged undeformed. The compression plate then applied a deformation width of 14% (9.8mm) in the x-direction, and the phantom was imaged again (after giving it about 30 seconds to settle in the new compression mode). The phantom was free to deform on the top and on the sides, but was constrained laterally (compression plate) and medially. This setup and the boundary conditions for the silicone phantom approximate quite well those of a real breast, expect that in the real case, the patient is in the prone position. However the phantom possesses enough integrity of shape that we can neglect the effect of gravity.
An axial and a coronal T1-weighted fast multi planar gradient echo (FMPGR) sequences were performed both in the uncompressed and compressed case. The sequences were performed with a repetition time (TR) of 325ms, a flip angle of 45$^{o}$ and an echo time (TE) of 3.4ms. The field of

view (FOV) in each slice was 140mmx140mm, with 2mm thick slices. The images were reconstructed to a 256x256 matrix, with a pixel size of 0.55mm.
The calculated dimensions of the phantom from the MR images agree within 1.6mm in the x-y plane (a maximum possible reported error of 3 pixels when measuring dimensions) and within 2mm in the z plane, with the physically calculated dimensions.

### 5.3 Material Properties

The elastic properties of the phantom materials were evaluated on an Instron Model 1331 (cambridge, MA) mechanical testing machine containing a semi-hydraulic computer driven system for very accurate tensile strength measurements.
Flat cylindrical samples of the silicone gel and the stiffer inclusion underwent uniaxial stress tests. Static load-deformation (stress-strain) curves were obtained.
The silicone gel can be assumed to be an isotropic hyperelastic material, and be described by a "strain energy potential" which defines the strain energy stored in the material per unit of reference volume. The experimental data was fit to a law of rubberlike material known as the Mooney-Rivlin strain energy function [16, 17]. We assume that the silicone gel is incompressible and temperature independent (in the conditions of the experiment).
The strain energy potential is thus given by: $U = C_{10} ( \boldsymbol{I_1} - 3) + C_{01} (\boldsymbol{I_2} - 3)$ (1)
Where $\boldsymbol{I_1} = \boldsymbol{\lambda_1}^2 + \boldsymbol{\lambda_2}^2 + \boldsymbol{\lambda_3}^2$ and $\boldsymbol{I_2} = \boldsymbol{\lambda_1}^{-2} + \boldsymbol{\lambda_2}^{-2} + \boldsymbol{\lambda_3}^{-2}$ are the first and second deviatoric strain invariants respectively, and $\boldsymbol{\lambda_i}$ are the deviatoric stretches. $C_{10}$ and $C_{01}$ are the material parameters to be determined experimentally. Because we assume incompressibility, and isothermal response, the total volume ratio J is equal to 1.
By invoking the principle of virtual work, we derive the nominal stress-strain relationship:
$T_U = \partial U / \partial \lambda_U$ where $T_U$ is the uniaxial nominal stress, and $\lambda_U$ is the stretch in the loading direction. After simplifying, rearranging the terms, and using the relation $\lambda_U = (\varepsilon_U+1)$ where $\varepsilon_U$ is the nominal strain, we finally get the equation:
$T_U = 2 [1-(\varepsilon_U + 1)^{-3}][ C_{01} + C_{10} (\varepsilon_U +1)]$ (2)
where $T_U$ and $\varepsilon_U$ are the uniaxial nominal stress and strain respectively.
Equation (2) was fit to the experimental stress-strain curves for the two types of silicone gel, using the least sum of squares method. The average parameter values calculated are:

| *Surrounding silicone gel in the phantom* | *Silicone gel inclusion* |
|---|---|
| $C_{10} = 3740 \pm 64$ N/m$^2$ | $C_{10} = 16300 \pm 815$ N/m$^2$ |
| $C_{01} = 1970 \pm 34$ N/m$^2$ | $C_{01} = 10490 \pm 524$ N/m$^2$ |

### 5.4 Deformable phantom model

The breast model was built using the *BreastView* software, and consists of 21 slices (each slice being in the x-y plane), stacked along the z-axis. The model was built from the axial MR data. Each slice is 4mm thick. The other model of the phantom was built directly from its physical dimensions using a pre-processor program MSC/PATRAN (MSC, CA), which automatically meshed the model, keeping 21 elements in the z-direction. The number of nodes in the x- and y-directions is 18 and 22 respectively, in order to have square shaped volume elements. Both finite element models were made of 7497 elements. The finite element modeling simulations were done using a robust finite element code ABAQUS/STANDARD V.5.8 (HKS, Rhode Island), commercially available.
Each finite element was modeled as a hybrid incompressible solid quadrilateral element, which allows a fully incompressible constraint at each material calculation point [18]. The element material properties were given a homogeneous, isotropic, Mooney-Rivlin hyperelastic model,

with the $C_{10}$ and $C_{01}$ constants as measured above. The boundary conditions were applied appropriately, and the 9.8mm displacement of the pressure plate was modeled in the initial conditions as a 9.8mm displacement constraint on every node which belongs to the displaced surface of the phantom.

# 6 Results and Discussion

## 6.1 MRI Imaging

The axial slice going through the center of the inclusion is shown in Fig. 5 in the uncompressed and in the compressed mode. As expected the edges of the phantom have changed shape as well as the edges of the tumor. Because silicon is incompressible, the side deformations of the phantom are quite large. Despite the high level of adhesion of the silicon phantom to its holding base, a little horizontal sliding occurred at the base, however we neglected this effect when measuring the displacement of the inclusion.
Because it is important in the real case to track the displacement of a cancer tumor in the breast, we tracked the displacement of the inclusion in the phantom. By using an image analysis software, we measured the displacement vectors of the center of the inclusion, as well its eight corners. We used the axial slices to measure the x and y displacements, and the coronal slices to measure the z displacements.

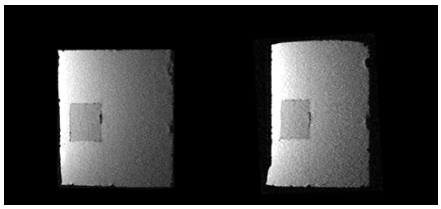

(a) (b)

**Fig. 5.** (a) Uncompressed, and (b) 14% compressed axial MR slice of phantom.

The displacement results are shown in Table 1.

| | 1 | 2 | 3 | 4 | 5 | 6 | 7 | 8 | center |
|---|---|---|---|---|---|---|---|---|---|
| x | 9.3 | 9.4 | 9.4 | 9.4 | 6.1 | 6.1 | 6.1 | 5.5 | 8.3 |
| y | 0.0 | 0.6 | 1.1 | 0.0 | 0.5 | 2.2 | 2.2 | 0.5 | 1.7 |
| z | 1.1 | 1.1 | -0.6 | -0.6 | 1.7 | 1.1 | -1.7 | -2.2 | 0.6 |

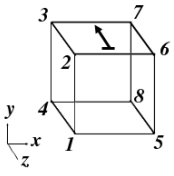


**Table 1.** Displacement vectors (mm) for the inclusion corners and center, from MR data.

### 6.2 Finite Element Model Simulations

A static displacement simulation was done on both PATRAN-generated and *BreastView*-generated models. Each simulation took about ten full hours on a Silicon Graphics Indigo workstation with 192Megs of RAM. Fig. 6 below shows the PATRAN-generated model after compression.

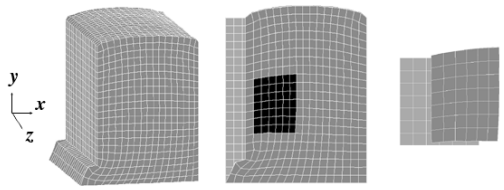


**Fig. 6.** (a) 3D view of PATRAN-generated model, (b) Axial slice through the center of the inclusion, (c) axial view of inclusion center, before and after compression.

Both model deformation results were extremely similar. We verified that the total energy of both models was conserved. The displacement vectors of the inclusion corners and center are shown for the *BreastView*-generated model in Table 2. Table 3 shows the difference between the displacements from the *BreastView*-generated model, the PATRAN-generated model, and the experimental displacement results. The last column in Table 3 represents the absolute average difference for each dimension.

| | 1 | 2 | 3 | 4 | 5 | 6 | 7 | 8 | center |
|---|---|---|---|---|---|---|---|---|---|
| x | 9.8 | 9.7 | 9.7 | 9.8 | 5.8 | 6.4 | 6.4 | 5.7 | 8.7 |
| y | 0.7 | 0.9 | 0.9 | 0.7 | 1.2 | 3.2 | 3.2 | 1.2 | 2.2 |
| z | 0.4 | 0.5 | -0.7 | -0.5 | 1.7 | 1.7 | -2.0 | -1.7 | 0.0 |

**Table 2.** Displacement vectors (mm) for the inclusion corners and center, from *BreastView* model.

| | Corner nb > | 1 | 2 | 3 | 4 | 5 | 6 | 7 | 8 | center | Avg. difference |
|---|---|---|---|---|---|---|---|---|---|---|---|
| x | with PATRAN | 0.0 | 0.0 | 0.0 | 0.0 | 0.0 | 0.1 | 0.1 | -0.1 | 0.1 | 0.04 |
| | With experimental | 0.5 | 0.3 | 0.3 | 0.4 | 0.2 | 0.4 | 0.4 | 0.2 | 0.4 | 0.34 |
| y | with PATRAN | -0.1 | 0.1 | 0.1 | -0.1 | -0.1 | -0.1 | -0.1 | -0.1 | -0.1 | 0.1 |
| | With experimental | 0.7 | 0.3 | -0.2 | 0.7 | 0.7 | 1.0 | 1.0 | 0.7 | 0.6 | 0.66 |
| z | with PATRAN | -0.2 | 0.0 | -0.2 | 0.1 | -0.5 | -0.4 | 0.1 | 0.5 | -0.2 | 0.3 |
| | With experimental | -0.7 | -0.6 | -0.1 | 0.1 | 0.0 | 0.6 | -0.4 | 0.5 | -0.6 | 0.4 |

**Table 3.** Displacement differences (mm) with the *BreastView* model displacement results, for each corner of the inclusion and center.

Table 3 indicates several interesting results. First of all it shows that the methodology used to create the phantom model using *BreastView* is sound since it results in a model which yields virtually the same inclusion displacement results as the PATRAN-generated model. We note that

the latter mentioned model was built directly from the measured dimensions of the phantom, therefore it can be considered as a reference against which to compare the other model. The very slight discrepancies ranging from 0.1mm to 0.5mm are well within the maximum reported error range and may be very well due to the not completely accurate segmentation process which precedes the generation of the 3D model mesh.
When comparing the deformable phantom model displacement results with the experimental displacements, the numbers show an average displacement difference in the y-direction (0.66mm) that is almost twice the difference in the x-direction (0.34mm). This is probably due to the small sliding effect of the phantom base after compression. Since the silicon gel phantom is virtually incompressible, this small sliding has caused the phantom to rise higher than expected in the y-direction (and also in the z-direction). This effect can also be seen when measuring the base to top deformation distance of the phantom in the central axial slice, which is +10mm for the experimental results, and +8mm for the deformable model.

## 7 Conclusion

This initial phantom study shows that it may be possible to create a deformable model of the breast based on the use of finite elements with non-linear material properties capable of modeling the deformation of the breast. The geometry of the model is constructed from MR data, and the material properties of the different structures are computed independently using material testing techniques.
The validation process for the finite element model is done using a real deformable silicone phantom, whose geometry can be easily controlled. The most important characteristic of the phantom is that it contains an inclusion (which models a breast tumor) whose center and edge deformation can be precisely tracked on its corresponding MR images.
Based on this methodology, the model will be further validated using a more complex deformable phantom, which approximates better the shape and tissue distribution of the breast. The simulation will be achieved by running the deformable model through an FEM software such as ABAQUS/STANDARD with the appropriate boundary and initial conditions. In this case, it will be necessary to model the compression plate with a rigid element the size of the plate. The contact interaction modeling capability of ABAQUS/STANDARD will allow the modeled compression plate to apply the same deformation to the phantom model, as in reality. From the deformed model, we will calculate the displacement vectors of the center of the inclusion as well as of its edges, and compare them to the measured displacements obtained from MR data, as we did here.
This deformable model will be used as a new tool to the physician, who will: 1) image the breast with no compression (thus increasing the contrast and visibility of the tumor), 2) use the compression plates (to minimize deformations caused by the insertion of the needle), 3) compress the breast model, and accurately locate the tumor within the real compressed breast.
This finite element model could also be used to register 3D data sets of the same breast from different imaging modalities. Another possible application of the model also involving registration, could be in mammography to register a Cranio-Caudal (CC), to a Medio-Lateral Oblique (MLO) X-ray image of the same breast, by appropriately applying the compressive plates to the 3D deformable model.

## References

1. Boring CC, S.T., Tong T, et al., *Cancer Statistics.* CA Cancer J Clin. 44 (1994) 7
2. Kuhl, C., *MRI of the Breast.* Advances in MRI Contrast 5(3) (1998) 56-69

3. Dash N, L.A., Daffner RH, Deep ZL, et al, *Magnetic resonance imaging in the diagnosis of breast disease.* AJR 146 (1985) 119
4. Kaiser WA, Z.E., *MR imaging of the breast: fast imaging sequences with and without Gd-DTPA. Preliminary Observations.* Radiology 170 (1989) 681
5. Heywang SH, H.D., Schmidt H, et al., *MR imaging of the breast using Gd-DTPA.* J Comput Assis Tomogr 10 (1986) 199
6. Heywang SH, W.A., Pruss E, et al., *MR imaging of the breast with Gd-DTPA: use and limitations.* Radiology 171 (1989) 95-103
7. Harms SE, F.D., Hesley KL, et al., *MR imaging of the breast with rotating delivery of excitation off resonance: clinical experience with pathologic correlation.* Radiology 187 (1993) 493-501
8. Morris EA, S.L., Dershaw DD, *MR imaging of the breast in patients with occult primary breast carcinoma.* Radiology 205 (1997) 437-440
9. Gilles R., G.J., Lucidarme O, et al, *Nonpalpable breast tumors: diagnosis with contrast-enhanced subtraction dynamic MR imaging.* Radiology 191 (1994) 625-631
10. Heywang-Koebrunner SH, H.M., Requardt H, et al, *Optimal procedure and coil design for MR imaging-guided transcutaneous needle localization and biopsy.* Radiology 193(P) (1994) 267
11. Egan R.L., *Breast Embryology, Anatomy and Physiology.* Breast Imaging: Diagnosis and Morphology of Breast Diseases (Chap. 4) (1988) 30-58
12. Egan R.L., *Malignant breast lesions.* Breast imaging: diagnosis and morphology of breast diseases (chap. 14) (1988) 227-231
13. *Understanding Breast Cancer Treatment.* National Cancer Institute NIH 98-4251 (1998) 6-7
14. Goldstein DC, K.H., Daube-Whiterspoon ME, Thibault LE, Goldstein EJ, *A silicone gel phantom suitable for multimodality imaging.* Invest Radiol 22 (1987) 153-157
15. Young A.A., A.L., Dougherty L., Bogen D.K., Parenteau C.S., *Validation of tagging with MR imaging to estimate material deformation.* Radiology 188 (1993) 101-108
16. Green A.E., Z.W., *Theoretical elasticity.* London, England: Oxford University (1968) 99
17. Spencer AJM, *Continuum mechanics.* London, England: Longman (1980) 153-163
18. ABAQUS/Standard V.5.8, *Hibbitt, Karlsson & Sorensen.* Vol. II (1998) 14.1.4-1, 14.1.4-17